A&A 461, 977–982 (2007)
DOI: 10.1051/0004-6361:20066146

Astronomy & Astrophysics

The stellar population of the Rosat North Ecliptic Pole survey⋆

G. Micela[1], L. Affer[1,2], F. Favata[3], J. P. Henry[4], I. Gioia[5], C. R. Mullis[6], J. Sanz Forcada[7], and S. Sciortino[1]

[1] INAF – Osservatorio Astronomico di Palermo, Piazza del Parlamento 1, 90134, Palermo, Italy
e-mail: giusi@astropa.inaf.it
[2] Dipartimento di Scienze Fisiche e Astronomiche – Università di Palermo, Piazza del Parlamento 1, 90134 Palermo, Italy
[3] Astrophysics Mission Division, RSSD of ESA/ESTEC, Postbus 299, 2200 AG Noordwjik, The Netherlands
[4] Institute for Astronomy, University of Hawai'i, 2680 Woodlawn Drive, Honolulu, HI 96822, USA
[5] INAF – Istituto di Radioastronomia INAF-CNR, via Gobetti 101, 40129, Bologna, Italy
[6] Department of Astronomy, University of Michigan, 918 Dennison Building, Ann Arbor, MI 48109-1042, USA
[7] LAEFF, European Space Astronomy Center, Apartado 50727, 28080 Madrid, Spain

Received 31 July 2006 / Accepted 10 October 2006

ABSTRACT

Context. X-ray surveys are a very efficient mean of detecting young stars and therefore allow us to study the young stellar population in the solar neighborhood and the local star formation history in the last billion of years.
Aims. We want to study the young stellar population in the solar neighborhood, to constrain its spatial density and scale height as well as the recent local star formation history.
Methods. We analyze the stellar content of the ROSAT North Ecliptic Pole survey, and compare the observations with the predictions derived from stellar galactic model. Since the ROSAT NEP survey is sensitive at intermediate fluxes is able to sample both the youngest stars and the intermediate age stars (younger than 10^9 years), linking the shallow and deep flux surveys already published in the literature.
Results. We confirm the existence of an excess of yellow stars in our neighborhood previously seen in shallow survey, which is likely due to a young star population not accounted for in the model. However the excellent agreement between observations and predictions of dM stars casts some doubt on the real nature of this active population.

Key words. stars: activity – stars: coronae – X-rays: stars – Galaxy: solar neighbourhood

1. Introduction

Stellar X-ray observations have shown that X-ray luminosity decreases by 3–4 orders of magnitude during the stellar life-time (see Favata & Micela 2003 for a recent review), with most of the evolution occurring during the main sequence life-time. This property makes X-ray surveys very effective in identifying young stars in the solar neighborhood, since they are detectable out to much larger distances than old stars, and are proportionally over-represented in X-ray flux limited surveys. Shallow soft X-ray surveys have previously been used to study some of the properties of young stellar populations, such as their density in solar neighborhood, and their spatial distribution and stellar birthrate in the last billion years (Favata et al. 1992; Micela et al. 1993; Tagliaferri et al. 1994; Guillout et al. 1996, 1998; Feigelson et al. 2004).

Early *Einstein* data allowed to study the young population thanks to the analysis of the *Extended Medium Sensitivity Survey* (EMSS, Gioia et al. 1990) where an excess with respect to model predictions of yellow stars was discovered (Favata et al. 1988; Sciortino et al. 1995). The youth of the detected population was confirmed by lithium abundance measurements (Favata et al. 1993). Similar results were found with EXOSAT (Tagliaferri et al. 1994), and with ROSAT both in EUV band (Jeffries & Jewell 1993) and in soft X-rays (Guillout et al. 1996).

Stellar X-ray surveys allow us to constrain the stellar birthrate in the last billion years, an age range that is very difficult to explore by means of different techniques (Micela et al. 1993; Guillout et al. 1996). For example, the cross correlation of ROSAT All Sky Bright survey sources and Tycho stars has evidenced a structure of young solar mass stars spatially coincident with the Gould Belt, likely related to a relatively recent episode of stellar formation in the solar neighborhood (Guillout et al. 1998).

X-ray surveys based on the presently operating observatories, *Chandra* and XMM/*Newton* give a different and unique contribution to the study of stellar populations since, thanks to their high sensitivity, they allow us to reach and go beyond the scale heights of the young stars. In fact, at the limiting sensitivity typical of deep *Chandra* and XMM/*Newton* observations, all the young stars within several hundreds of parsecs will be detected. Since the scale height of young (and even intermediate age) stars is less than 200 parsecs, deep observations at high galactic latitude will detect all the young stars in the field of view. Deeper observations will only result in the detection of additional intrinsically X-ray faint old stars, which also have a spatial distribution with a larger scale height. Such observations permit us to investigate in the X-ray regime the old stellar population, easily separating it from the younger stars. This has been, for example, the subject of Feigelson et al. (2004) who studied the stellar content of the *Chandra* Deep Field North. Stars detected in such deep surveys are expected to be several billion years old,

⋆ Tables 1 and 2 are only available in electronic form at http://www.aanda.org

and their observed number suggests a substantial decline of X-ray activity beyond 1 billion years in age.

In this context the ROSAT North Ecliptic Pole survey plays a relevant role, since its sensitivity is intermediate between that of the EMSS (sensitive at fluxes $\sim 10^{-13}$ erg cm^{-2} s^{-1}) and the surveys being performed with *Chandra* or XMM/*Newton* (sensitive at fluxes $\sim 10^{-15}$ erg cm^{-2} s^{-1}). The EMSS (and most of the RASS) is quite shallow and, as discussed above, detected preferentially young stars, while *Chandra* and XMM/*Newton* surveys, being very sensitive, will be dominated by old stars (Micela 2003). The NEP survey with its moderately deep sensitivity, (fluxes $\sim 10^{-14}$ erg cm^{-2} s^{-1}) is able to sample the intermediate-age (10^8–10^9 years) population. Furthermore it has the unique characteristics of covering a relatively large contiguous area of the sky.

The present paper is structured in the following way: in Sect. 2 we present the X-ray observations and optical data, in Sect. 3 we summarize the stellar properties of NEP stars, while in Sect. 4 we compare observations with predictions of our model.

2. Stellar data

2.1. X-ray data

The ROSAT North Ecliptic Pole Survey (NEP, Henry et al. 2001, 2006), covers a 9° × 9° area centered on the North Ecliptic Pole (RA(J2000) = $18^h00^m00^s$, Dec(J2000) = +66°33′39″, l = 96.°4, b = 29.°8), which is the sky region observed with the highest sensitivity during the ROSAT All Sky Survey (RASS), with exposure times up to ∼40 ks at the pole. The galactic latitude (b = 29.8°) together with the moderate sensitivity allow us to observe young stars close to their scale height and to study their spatial distribution.

The data analysis processing is described in Voges et al. (1999, 2001) and Mullis (2001). The detection algorithm was applied to the *ROSAT* energy band 0.1–2.4 keV, producing a total of 445 sources with likelihood of existence $L \geq 10$, where $L = -\ln(P)$ and P is the probability that the source does not exist (count rate = 0). With this choice ∼2 spurious sources are expected.

Optical follow up observations were obtained and all but two NEP sources were identified (Gioia et al. 2003). The identification procedure is based on spectroscopic observations, or inspection of finding charts together with analysis of literature data on possible counterparts falling in the error circle of the X-ray source until a likely optical counterpart is identified (see Gioia et al. 2003 for a detailed description of the adopted procedure).

More than half of the sources are identified with AGN, about one third with stars and about 15% with clusters of Galaxies. The extragalactic component is discussed extensively in Mullis et al. (2003, 2004a,b), Gioia et al. (2004), and Henry (2006). Here we analyze in detail the properties of the 152 identified stellar counterparts.

2.2. Optical data and observations

Our sample is made of the 152 ROSAT NEP X-ray sources with stellar counterparts. For our analysis we need to determine spectral types, in order to determine the properties of this active stellar population. As a first step we have searched for possible counterparts in SIMBAD, looking for spectral types and stellar properties. In total 37 sources have as counterparts stars in SIMBAD with spectral types while further 17 stars have $B - V$ colors, that may be used to have a first estimate of their nature. All 152 stellar sources have been matched with the 2MASS catalog (Cutri et al. 2000) and only 4 sources with very faint counterparts in the POSS have no 2MASS counterparts.

In order to assess the nature of NEP sources Gioia et al. (2003) obtained spectra of a fraction of the stellar sources. Their spectroscopic observations were taken at the UH 2.2 m Wide-Field Grism Spectrograph (WFGS) and Multi-Object-Spectrograph (MOS) at CFHT 3.6 m and the Low-Resolution Imaging Spectrograph (LRIS) on the Keck telescope. In order to complete the spectral classification of the sample we have taken spectra of 75 counterparts of 67 X-ray sources including stars with only $B - V$ colors in Simbad. We have reobserved also a sample of stars with spectra already available to have an homogeneous classification sample. Low-resolution spectra were acquired on 2004 June 10 and 11, using ALFOSC[1] in its spectroscopic mode, with the 2048 × 2052 CCD8 at the f/11 focus of the NOT telescope, with a pixel size of 13.5 μm and a scale of 0.″19 pixel^{-1}. We used the 600 mm^{-1} red grism and the 1.″0 slit, which provided a pixel scale in spectroscopic mode of 1.3 Å pixel^{-1}, a spectral resolution of ≈4.8 Å *FWHM*, and a wavelength coverage of approximately 5825–8350 Å. Exposure times ranged from 10 s to 700 s, resulting in S/N ratios per pixel averaging at about 70. A spectrum of a He+Ne lamp was obtained following each stellar spectrum, ensuring accurate wavelength calibration.

The optical data were analyzed using standard IRAF[2] reduction packages. A first, fast reduction and interpretation of long-slit spectra was normally completed in "real-time" at the telescope (in order to decide if further spectra were required to make a reliable classification) with the task "QuickSpec", which detects and automatically reduces the brightest source on the slit. Nevertheless, all data were subsequently reduced off-line using standard procedures. The analysis includes bias subtraction, flat-fielding, removal of scattered light and wavelength calibration. For each star we acquired from two to six consecutive exposures which were combined, with the IRAF task SCOMBINE, rejecting pixels exceeding specified low and high thresholds and computing the weighted average of the remaining pixels in order to build an average, low-noise spectrum.

Spectra were classified according to the presence or absence of various absorption lines and to the shape of the continuum emission by comparison with standard objects. With this aim we also acquired, with the same instrumental set-up as the NEP survey spectra, the spectra of 25 standard stars which are reported in Table 1, together with their spectral types and references. Examples of typical spectra for three different spectral types are reported in Fig. 1. Note the appearance of molecular bands and of the Hα emission line in the spectrum of the dM star.

3. Results

We have determined the spectral types for all 152 sources. Table 2 reports the 2MASS photometry and spectral type for our sample. Our classification is accurate at 1–2 subspectral

[1] The data presented here have been taken using ALFOSC, which is owned by the Instituto de Astrofisica de Andalucia (IAA) and operated at the Nordic Optical Telescope under agreement between IAA and the NBIfAFG of the Astronomical Observatory of Copenhagen.

[2] IRAF (Image Reduction and Analysis Facility) is distributed by National Optical Astronomy Observatories, operated by the Association of Universities for Research in Astronomy, Inc., under cooperative agreement with the National Science Foundation.

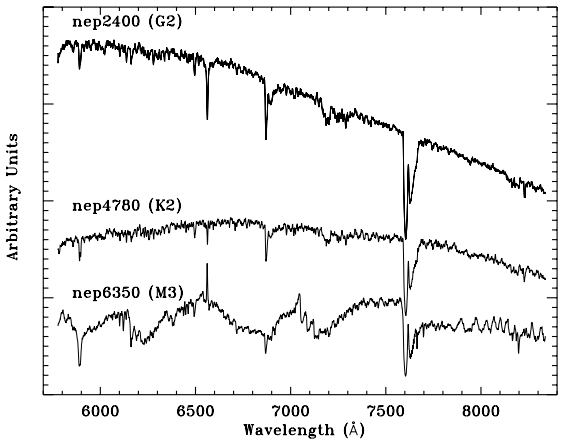

Fig. 1. Examples of typical spectra for different spectral types obtained with the NOT telescope.

type, sufficient for our aims. Only in two cases the signal to noise is low and allows us only a rougher estimates. The source RX J1824.7+6509 is extragalactic, although in Gioia et al. (2004) was identified as a star (see also Mullis et al. 2004a), for this reason in the following we exclude it from the sample. Seven sources are peculiar stars (Be, CV, WD) and will not be discussed in the following. Summarizing, we are left with a sample of 144 sources identified with "normal stars".

A summary of the spectral type classification is reported in Table 3. We have separated spectral type F in two subsamples since early-F stars are expected to share X-ray characteristics with A stars, with very shallow, if any, convection zone that may drive a solar-like dynamo, while the internal structure of late-F stars is more similar to that of dG stars. This different internal structure is expected to produce different level coronal emission, with late-F and dG stars brighter in X-rays than A and early-F stars. The chosen grouping make also easier the comparison with models (Sect. 4) that use X-ray luminosity functions in the solar neighborhood, commonly computed for late-F and dG stars together (i.e. Maggio et al. 1987). As expected from the volume limited nearby population, most ($\sim 2/3$) of the detected stars are K-M stars, $\sim 1/4$ are solar-like stars, and only less than 10% are A and early-F stars.

4. Model predictions and comparisons with the observations

4.1. Modeling of the stellar content of the ROSAT NEP survey

We have analyzed the properties of the ROSAT NEP X-ray stellar population using our model XCOUNT (Favata et al. 1992; Micela et al. 1993). The model assumes an exponential disk-like spatial distribution of the stars, with a radial scale length of 3.5 kpc, as in Bahcall & Soneira (1980). We have modified the Bahcall & Soneira (1980) model by introducing an age-dependent scale height. We divide stars in three age ranges: 10^7–10^8, 10^8–10^9, and 10^9–10^{10} years, with scale heights of 100, 200, and 400 pc, respectively. For each spectral type and age range we have assumed X-ray luminosity functions derived from ROSAT observations of the Pleiades (Micela et al. 1996) and Hyades (Stern et al. 1995), and from *Einstein* data for nearby stars (Schmitt et al. 1985; Maggio et al. 1987; Barbera et al. 1993), considered as prototypes of the three age ranges. We assume also that the average coronal temperature decays with age, assuming 1.0 keV for Pleiades (Gagne et al. 1995), 0.5 keV for Hyades (Stern et al. 1995) and 0.3 keV for old stars (Schmitt et al. 1985). We predict also the expected giants assuming the X-ray luminosity from Pizzolato et al. (2000) and RS CVns using the X-ray luminosity function derived from data of Dempsey et al. (1997). XCOUNT uses the distribution of interstellar matter from Lockman (1984).

Table 3. Summary of spectral type classification of stellar X-ray NEP sources.

Sp.Type	N. Obs.
A	3
F-F5	10
F6-F9	8
G	29
K	53
M	41
Tot.	144

Table 4. Summary of X-ray source counts predictions for each spectral type and range of age derived from XCOUNT.

Sp. Type	*N*(young)	*N*(intermed.)	*N*(old)	Total
A	0.63	1.41	0.28	2.32
F-F5	0.32	1.53	7.34	9.18
F6-F9+G	1.91	8.42	7.63	17.95
K	4.24	8.86	20.26	33.35
M	9.38	22.2	10.07	41.35
	16.42	42.26	45.48	104.16

In order to predict X-ray source counts we have used the sensitivity map binned in sensitivity for a total of 14 400 regions ranging between 17 and 24 arcmin square as computed for the NEP analysis (Voges et al. 2001; Henry et al. 2006). The sensitivity ranges between 2×10^{-3} and 1.6×10^{-2} cnt/s. We prefer to use a sensitivity map expressed in cnt/s rather than in flux because stars of different age may have different dominant coronal temperatures, and therefore X-ray spectra, producing a non-unique transformation between cnt/s and flux. The predictions are computed separately for each sensitivity region and summed up.

We have compared the number of detected stars and their properties with those predicted with the XCOUNT model (Favata et al. 1992; Micela et al. 1993). The comparison between the observations and the predictions gives us important information on the detected star population and allows us to constrain some of the parameters of the model.

4.2. Model results

The predictions of our modeling in the ROSAT NEP survey for each spectral type and age range are summarized in Table 4, and shown in Figs. 2 and 3. In addition to the 104 "normal" main sequence stars our model predict 0.8 giant stars and a number of RSCVn systems in the range between 3.8 and 14.7, corresponding to a total number between 108 and 119 predicted stellar sources. The exact number of predicted RSCVns depends on the assumed spatial density, which still is not firmly established. The above range is derived assuming the minimum and maximum estimated density for this stellar population (Favata et al. 1995). Although we have computed the expected number both for high and low density of binary systems, previous work (Favata et al. 1995) has shown that the actual density is closer to the low limit than the higher one.

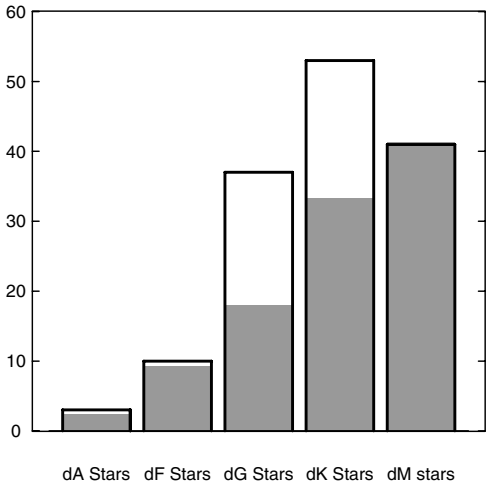

Fig. 2. Spectral type distribution of the stellar population of the NEP stars predicted with XCOUNT (shaded histogram). Empty hystogram marks the actual observed stars.

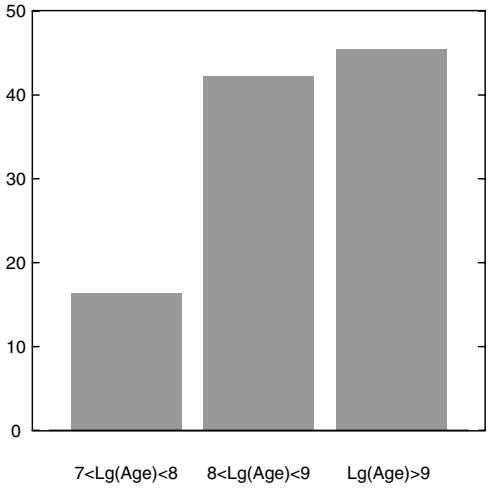

Fig. 3. Age distribution of the stellar population of the NEP stars predicted with XCOUNT. The predicted stellar population is equally dominated by intermediate-age and old stars.

The sample is expected to be dominated by dK and dM stars of intermediate and old age. In particular the dK sample should be dominated by old stars, while the dM sample is mainly composed of intermediate Hyades-like age stars. We show the contribution of the samples of stars of different age to the stellar $\log N - \log S$ in Fig. 4. Vertical dashed lines mark the range of limiting sensitivity of our survey. The plot shows that, while the $\log N - \log S$ of the oldest stars is approximately a power law with a slope of about 3/2, as expected for a spherically distributed population as we are not reaching stars outside the disk, the $\log N - \log S$ of the youngest populations deviate from the power law. In practice their low scale height together with their high X-ray luminosity determine a count rate beyond which no new stars are observed as the limiting distance falls outside the disk. The figure shows that the NEP survey is too shallow to be sensitive to this effect. At the NEP sensitivity even the young populations are almost spherical distributed so that their $\log N - \log S$ is sensitive mainly to spatial star density. In a similar way Fig. 5 reports the contribution of different spectral types.

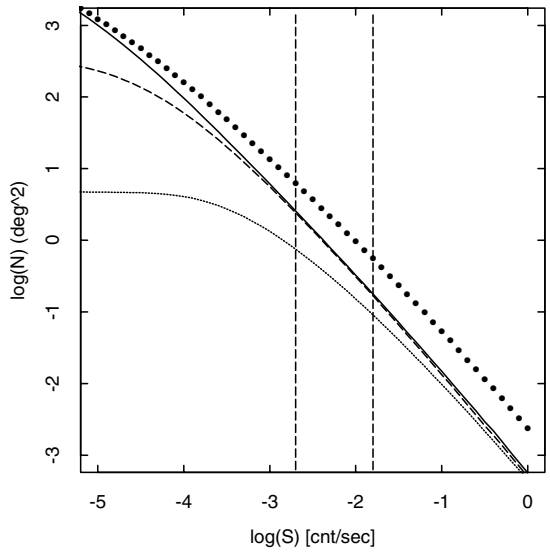

Fig. 4. Log $(N)-$Log (S) predicted with *XCOUNT* toward the NEP. Flux is expressed in ROSAT/PSPC count rate. Short dashed, long-dashed, and solid lines are the contributions of young, intermediated and old stars, respectively. Vertical dashed lines mark the range of limiting sensitivity of the survey. At the NEP sensitivity, intermediate and old populations dominate the stellar sources. At higher fluxes also the youngest stars give a large contribution, while at faint fluxes the stellar population is largely dominated by oldest stars.

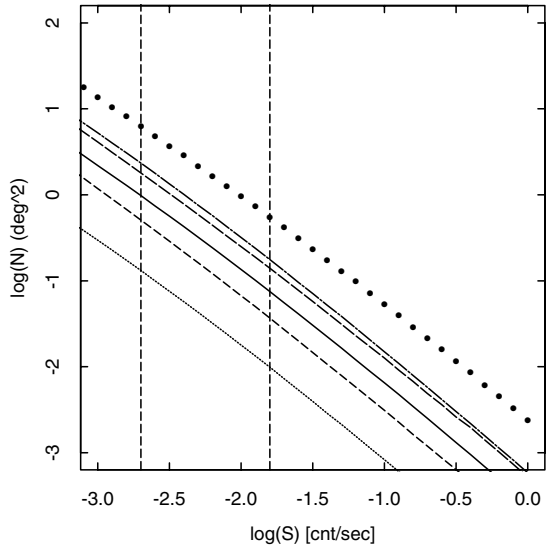

Fig. 5. Log $(N)-$Log (S) predicted with *XCOUNT* toward the NEP. Flux is expressed in ROSAT/PSPC count rate as in Fig. 4. Figure shows the contribution from dA, dF, dG, dK, and dM stars (going from the lower contribution to the the largest). Vertical dashed lines mark the range of limiting sensitivity of the survey.

4.3. Comparison with the observations

Our model predicts a total of 108 (119 if we assume the high spatial density for active binary population) detected stars to be compared with 144 observed stars. In particular, the observations and the predictions for A and early F stars are in excellent agreement (11.5 predicted and 13 observed), as are dM stars (41.35 predicted and 41 observed), while the difference is concentrated among dG and dK stars (51.3 predicted and 82 observed) The NEP survey therefore confirms the presence of an excess of yellow stars in shallow X-ray surveys. This is

evident from Fig. 2, where the empty hystogram marks the number of observed stars while the filled histogram represents the model predictions.

The excess of detected active stars in shallow X-ray surveys has been attributed to a young population in the solar neighborhood, not accounted for by the models (e.g. Sciortino et al. 1995). The detection of the lithium line in the optical spectra of such stars has been interpreted as a confirmation of such hypothesis (Favata et al. 1993). The alternative explanation, that active old binaries could be the responsible for the observed excess, is not supported by the optical spectroscopic observations.

However the explanation in terms of young stars is not completely satisfactory since it does not explain why the effect is concentrated among G and K stars. The decay of L_x with age is not a strong function of mass, therefore if a young population is present the excess should be observed also among M stars. This is not the case, and on the contrary, the observed dM stars appear to be in "perfect" agreement with the model in most of the X-ray surveys (see e.g. Micela 2003) and the discrepancy is always concentrated among yellow stars, with an observed excess in shallow surveys and a lack in deep surveys (Feigelson et al. 2003).

To better explore the characteristics of the observed discrepancy we may compare the expected and observed $\log N - \log S$, reported in Fig. 6. The observed $\log N - \log S$ shows an excess concentrated on rates larger than 0.01 cnt/s. For weaker fluxes the observations agree very well with the predictions. Such behavior is consistent with the presence of an active small scale height population, not accounted for by the model. High activity and small scale height are typical of a young population, however the bending of the $\log N - \log S$ appears at fluxes higher than those where the bending of a young (10^7–10^8 years) population is expected (10^{-2} cnt/s to be compared with 10^{-3} cnt/s, see Fig. 4, dotted line). A population responsible for this bending should have either an intrinsic X-ray luminosity one order of magnitude higher than the youngest population accounted for in our model (age 10^7–10^8 years), or a scale height ∼3 times smaller than this young population. Furthermore its density should be 1.5–2 times the density of the youngest stars, and concentrated on yellow spectral types (in addition to the RSCVn population, much less dense, already taken into account). We notice that is very difficult to justify the presence of a population with such characteristics (in particular the very small scale height), as it should have been easily detected in the nearby volume limited surveys of stellar X-ray emission (Maggio et al. 1987; Schmitt & Liefke 2004). Also, this hypothesis, as discussed below, appears in contradiction with the observed agreement between predictions and observations for the M stars.

In order to better understand the nature of this "excess" population we may take advantage of the relatively large number of stars in the ROSAT NEP survey and separately explore the behavior of the different spectral types. In Fig. 6 we have grouped together A and early F stars, G and K stars and dM stars. The earliest types contribute very little to the global $\log N - \log S$ but an excess is present at very high fluxes. It is possible that our survey is picking up a few very active, peculiar dA stars. At the same time dM stars appear in excellent agreement with the prediction essentially in all the explored flux range, while yellow stars seem in excess at every flux. In the light of these considerations, the bending of the observed total $\log N - \log S$ seems an artifact, due to a combination of a simultaneous small deficiency of dM stars at faint fluxes, and a minor excess of the yellow stars at faintest fluxes. Likely neither of these effects are

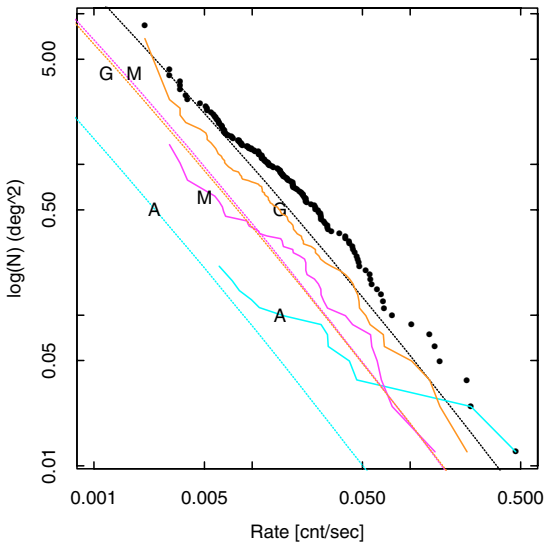

Fig. 6. Observed and predicted Log (N) – Log (S) toward the NEP. Flux is expressed in ROSAT/PSPC count rate as in Fig. 5. The upper line is the total expected $\log N - \log S$ and the points are the observations. The lower line represents the predictions for A and early F(label "A") stars, while the two dotted overimposed lines are the predictions for G-K and dM stars, respectively (labels "G" and "M"). The observed A and early F stars are marked by the lower irregular line, while observed dM stars are the intermediate irregular line, and the upper one is the observed $\log N - \log S$ of dG and dK stars.

significant. The observed excess is evenly distributed on the entire flux range, making implausible the hypothesis that an active, small scale height population, is responsible for the excess. An alternative hypothesis is that one is observing a moderately active population with a scale height ≥100 pc. X-ray stellar surveys have already identified the young low-mass stellar population of the Gould Belt or Disk (Guillout et al. 1998) associated to a recent star formation episode close to the Sun not accounted for in our galactic model. The NEP surveyed area is far from the Gould Belt, but it is possible that other local, less prominent events of star formation occurred in the solar neighborhood.

Therefore, while the hypothesis of a young population remains the most plausible, the lack of observed excess dM stars is not explained. The possibility remains that the identification process misses some of the optically fainter dM stars. In this case we should miss about 20 dM stellar identification from the entire NEP survey. Of course this would imply the very unlikely circumstance that about 20 NEP sources identified with an extragalactic sources are misidentified. At the same time, for this explanation to be valid, this would imply that the same identification bias is present in all shallow X-ray survey studied to date with a similar approach. An alternative explanation is that the X-ray luminosity functions of young and intermediated-age dM stars, based on Pleiades and Hyades, are biased toward high luminosity values. Such explanation is not implausible since the member catalogs may be uncomplete at the very low mass end, where the faintest X-ray stars belong.

Alternatively and more likely, a substantial fraction of binaries could be present in the detected sample. In this case we may have a yellow primary, that dominates the optical emission, and a dM companion that dominates the X-ray emission. In this case we observe an excess concentrated at yellow stars, although it is due both to solar and low mass stars. The effect could be particularly important if the fraction of binaries is larger in young stellar

population. Patience et al. (1998) for example, studying Taurus, Hyades and nearby star samples, find that the companion star fraction (considering mass ratio ~0.2−1.0 and separations in the 5–50 AU ranges) decreases from 0.4 to 0.15 for age increasing from 10^6 yr to 5×10^9 yr. The observed trend may depend on the specific environmental conditions of star formation, therefore it is not straightforward to interpret it exclusively as an evolutionary effect. However a detailed study of the fraction of binary systems in our sample is needed to address this hypothesis.

5. Summary and conclusions

We have analyzed the stellar content of the RASS North Ecliptic Pole survey, in order to determine the nature of active stars in the solar neighborhood. In particular we have determined the spectral types for the entire sample and have compared the observations with the predictions obtained with the XCOUNT model. Our analysis confirms the results obtained with previous moderately deep surveys, i.e. that an excess of active yellow stars is present in the nearby active stellar population.

The most plausible explanation of such excess is the presence of a young population, due to a relatively recent burst of star formation. Such hypothesis is supported by previous lithium detection in stars selected with analogous surveys. At the same time the X-ray spectral analysis of the stars detected by the XMM-*Newton* Bright Serendipitous Survey (Della Ceca et al. 2004) show that coronal plasma responsible for the emission is dominated by temperature typical of young or intermediate age stars (Lopez Santiago et al. 2006). Furthermore we note that one star of our sample (RX J1721.1+6947), coincident with HD 158063 has also an IRAS counterpart and it is included in the sample of Suchov et al. (2002) as candidate pre-main sequence F stars with circumstellar dust, implying youth.

However the explanation of the observed excess in terms of young stars is not completely satisfactory since we do not observe such excess among dM stars where it should be present if one were actually observing a young population. A possible explanation of such lack of excess could be that there is a substantial incompleteness of the stellar identifications of the sample (i.e. further 30 NEP sources should be faint stars in order to produce an excess in M stars equivalent to the excess observed in yellow stars) or that a significant fraction of binaries, with a low mass companion, is present among X-ray active stars. It remains however puzzling that in all the X-ray surveys studied to date, both shallow and deep, the detections of dM stars are remarkably in agreement with the model.

Further studies of the detected population, kinematics analysis, spectroscopic observations but also far infrared observations to detect the presence of residual dust disks around our stars, are needed to definitely assess the nature of this population that could trace the recent star formation history in the solar neighborhood.

Acknowledgements. Based on observations made with the Nordic Optical Telescope, operated on the island of La Palma jointly by Denmark, Finland, Iceland, Norway, and Sweden, in the Spanish Observatorio del Roche de los Muchachos of the Instituto de Astrofisica de Canarias. This publication makes use of data products from the Two Micron All Sky Survey (2MASS), which is a joint project of the University of Massachussetts and the Infrared Processing and Analysis Center/California Institute of Technology, funded by the National Aeronautics and Space Administration and the National Science Foundation. We acknowledge Javier Lopez Santiago for fruitful discussions. This work is part of the project ISHERPA funded by the European Commission (contract No. MTKD-CT-2004-002769).

References

Bahcall, J. N., & Soneira, R. M. 1980, ApJS, 44, 73
Barbera, M., Micela, G., Sciortino, S., Harnden, F. R., & Rosner, R. 1993, ApJ, 414, 846
Cutri, R. M., et al. 2000, Explanatory Supplement to the 2MASS Second Incremental Data Release (Pasadena: IPAC/Caltech)
Della Ceca, R., Maccacaro, T., Caccianica, A., et al. 2004, A&A, 428, 383
Dempsey, R. C., Linsky, J. L., Fleming, T., & Schmitt, J. H. M. M. 1997, ApJ, 478, 358
Favata, F., & Micela, G. 2003, Space Sci. Rev., 108, 577
Favata, F., Rosner, R., Sciortino, S., & Vaiana, G. S. 1988, ApJ, 324, 1010
Favata, F., Micela, G., Sciortino, S., & Vaiana, G. S. 1992, A&A, 256, 86
Favata, F., Barbera, M., Micela, G., & Sciortino, S. 1993, A&A, 277, 428
Favata, F., Micela, G., & Sciortino, S. 1995, A&A, 298, 482
Feigelson, E. D., Hornschemeier, A. E., Micela, G., et al. 2004, ApJ, 611, 1107
Gagne, M., Caillault, J.-P., & Stauffer, J. R. 1995, ApJ, 450, 217
Gioia, I. M., Maccacaro, T., Schild, R. E., et al. 1990, ApJS, 72, 567
Gioia, I. M., Henry, J. P., Mullis, C. R., et al. 2003, ApjS, 149, 29
Gioia, I. M., Wolter, A., Mullis, C. R., et al. 2004, A&A, 428, 867
Gould, A., Bahcall, J. N., & Flynn, C. 1997, ApJ, 482, 913
Guillout, P., Haywood, M., Motch, C., & Robin, A. C. 1996, A&A, 316, 89
Guillout, P., Sterzik, M. F., Schmitt, J. H. M. M., et al 1998, A&A, 334, 540
Henry, J. P., Gioia, I. M., Mullis, C. R., et al. 2001, ApJ, 553, L109
Henry, J. P., Mullis, C. R., Voges, W., et al. 2006, ApJS, 162, 304
Jacoby, G. H., Hunter, D. A., & Christian, C. A. 1984, ApJS, 56, 257
Jeffries, R. D., & Jewell, S. J. 1993, MNRAS, 264, 106
Lopez Santiago, J., Micela, G., Sciortino, S., et al. 2006, A&A, submitted
Maggio, A., Sciortino, S., Vaiana, G. S., et al. 1987, ApJ, 315, 687
Micela, G. 2003, Astron. Nachr., 324, 77
Micela, G., Sciortino, S., & Favata, F. 1993, ApJ, 618, 412
Micela, G., Sciortino, S., Kashyap, V., Harnden, F. R., & Rosner, R. 1996, ApJS, 102, 75
Micela, G., Sciortino, S., Harnden, F. R., Jr., et al. 1999, A&A, 341, 751
Mullis, C. R. 2001, Ph.D. Thesis, University of Hawaii
Mullis, C. R., McNamara, B. R., Quintana, H., et al. 2003, ApJ, 594, 154
Mullis, C. R., Henry, J. P., Gioia, I. M., et al. 2004a, ApJ, 617, 192
Mullis, C. R., Vikhlinin, A., Henry, J. P., et al. 2004b, ApJ, 607, 175
Patience, J., Ghez, M., Reid, I. N., Weinberger, A. J., & Matthews, K. 1998, AJ, 115, 1972
Pizzolato, N., Maggio, A., & Sciortino, S. 2000, A&A, 361, 614
Schmitt, J. H. M. M., & Liefke, C. 2004, A&A, 417, 651
Schmitt, J. H. M. M., Golub, L., Harnden, F. R., et al. 1985, ApJ, 290, 307
Sciortino, S., Favata, F., & Micela, G. 1995, A&A, 296, 370
Suchkov, A. A, Schultz, A. B., & Lisse, C. M. 2002, ApJ, 570, L29
Stern, R. A., Schmitt, J. H. M. M., & Kahabka, P. T. 1995, ApJ, 448, 683
Tagliaferri, G., Cutispoto, G., Pallavicini, R., Randich, S., & Pasquini, L. 1994, A&Ap, 285, 272
Voges, W., Aschenbach, B., Boller, Th., et al. 1999, A&A, 349, 389
Voges, W., Henry, J. P., Briel, U. G., et al. 2001, ApJ, 553, L119

Online Material

Table 1. Standard stars used in our spectral classification.

Star	Spectral type	Spectral type References
HD 78277	G2 IV	(1)
HD 237822	G3 V	(2)
SAO 81292	M4.5 Ve	(1)
HD 104979	G8 IIIa	(2)
HD 101501	G8 V	(2)
HD 113226	G8 III	(2)
HD 112872	G6 III	(1)
HR 6511	A1 Vn	(2)
HR 6826	B9 IIIn	(2)
HD 201092	K7 V	(2)
HD 219134	K3 V	(2)
HD 5351	K4 V	(1)
BD 63 0137	M1 V	(1)
HD 196755	G5 IV	(2)
HD 2506	G4 III	(1)
SAO 55164	K0 III	(1)
HD 4628	K2 V	(2)
HD 6111	F8 V	(1)
HD 10032	F0 V	(1)
HD 10476	K1 V	(2)
HD 70178	G5 IV	(1)
HD 66171	G2 V	(1)
HD 83140	F3 IV	(1)
HD 110964	M4 III	(1)
HD 210027	F5 V	(2)

(1): Jacoby et al. (1984).
(2): SIMBAD database, operated at CDS, Strasbourg, France.

Table 2. 2MASS photometry and spectral types for our sample. Names and scan numbers are from Gioia et al. (2003).

Name	Scan	RA(J2000) (h m s)	Dec(J2000) ° ′ ″	*J*	*H*	*K*	Sp.	Note
RX J1715.6+6856	1240	17 15 41.7	+68 56 43				Be†	G
RX J1715.6+6231	1241	17 15 42.3	+62 31 27	10.954	10.564	10.474	G5	G
RX J1718.3+6754	1350	17 18 19.6	+67 54 17	12.078	11.425	11.279	M3e	G
RX J1719.0+6852	1400	17 19 00.9	+68 52 32	11.273	10.686	10.441	M3	N
RX J1719.4+6522	1420	17 19 28.8	+65 22 29	10.034	9.602	9.516	K0	N
RX J1720.0+6206	1441	17 20 05.6	+62 06 22	7.973	7.633	7.571	G2	N
RX J1720.4+6703	1470	17 20 26.7	+67 03 37	8.752	8.383	8.317	G8	N
RX J1721.1+6947	1500	17 21 10.9	+69 48 02	6.117	5.746	5.682	G2	N
RX J1721.7+6200	1511	17 21 42.5	+62 00 32	9.555	9.054	8.921	K4	N
RX J1723.3+6333	1541	17 23 17.9	+63 33 26	11.286	10.681	10.488	M4e	G
RX J1724.0+6940	1580	17 24 00.4	+69 40 30	10.102	9.716	9.602	K2	N
RX J1724.4+6412	1600	17 24 26.8	+64 12 23	9.167	8.854	8.794	G2	N
RX J1724.6+6440	1601	17 24 38.8	+64 40 51	8.918	8.623	8.582	G0	N
RX J1726.7+6937	1690	17 26 45.4	+69 37 53	9.778	9.530	9.494	G2	N
RX J1727.9+6210	1741	17 27 56.6	+62 10 54				K	G
RX J1729.0+6529	1781	17 29 00.2	+65 29 52	11.516	11.004	10.889	K2	G
RX J1729.6+6847	1800	17 29 39.4	+68 47 38	8.335	8.168	8.147	F5	N
RX J1729.7+6737	1810	17 29 46.1	+67 38 13				M6	G
RX J1730.1+6247	1820	17 30 08.4	+62 47 55	15.284	15.189	15.217	CV†	G
RX J1730.3+6955	1840	17 30 19.9	+69 55 27	8.913	8.635	8.498	G0	N
RX J1733.2+6712	1960	17 33 16.9	+67 12 08	6.836	6.672	6.627	F2	S
RX J1736.2+6502	2050	17 36 14.1	+65 02 27	9.099	8.561	8.414	K0	S
RX J1736.4+6820	2100	17 36 26.6	+68 20 37	5.335	4.766	4.548	M3	S
RX J1736.9+6845	2130	17 36 57.0	+68 45 12	3.826	3.696	3.620	F5	S
RX J1738.0+6653	2132	17 38 02.3	+66 53 47	15.303	15.604	15.454	PN†	G
RX J1738.0+6314	2150	17 38 01.3	+63 14 22	10.044	9.526	9.353	K5e	N
RX J1738.0+6509	2170	17 38 04.4	+65 09 32	10.566	9.993	9.734	M4e	G
RX J1739.2+7020	2210	17 39 16.1	+70 20 09	8.047	7.809	7.763	F8	S
RX J1739.9+6500	2250	17 39 56.1	+65 00 04	6.767	6.302	6.190	K0	S
RX J1740.7+6255	2290	17 40 44.6	+62 55 12	10.804	10.129	9.965	M0e	N
RX J1742.4+6907	2360	17 42 26.5	+69 07 58	7.526	7.298	7.247	F8	N
RX J1742.5+6709	2370	17 42 33.8	+67 09 23	10.457	9.978	9.833	K3	N
RX J1743.0+6606	2400	17 43 01.6	+66 06 46	8.519	8.206	8.145	G2	N
RX J1743.8+7031	2470	17 43 51.7	+70 31 39	9.516	9.324	9.264	F3	N
RX J1744.0+7015	2480	17 44 00.6	+70 15 27	9.458	9.041	8.927	K0	N
RX J1744.5+6316	2510	17 44 32.3	+63 16 33	12.913	12.499	12.466	G2	G
RX J1745.2+6609	2551	17 45 12.1	+66 09 41	11.957	11.319	11.140	M4e	G
RX J1745.4+6918	2580	17 45 24.5	+69 18 21	10.243	9.678	9.540	K4	N
RX J1745.6+6543	2600	17 45 41.3	+65 43 49	11.517	10.970	10.837	K7e	N
RX J1746.2+6627	2740	17 46 15.1	+66 27 48	11.511	10.899	10.763	K3e	G
RX J1746.7+7047	2780	17 46 44.8	+70 47 03	10.757	10.103	9.963	M3e	G
RX J1748.4+6335	2920	17 48 29.3	+63 35 51	15.680	15.136	14.948	K	G,N
RX J1748.5+6308	2931	17 48 33.7	+63 08 45	11.224	10.829	10.753	G2	G
RX J1749.0+6247	2970	17 49 03.9	+62 47 48	5.932	5.809	5.754	F2	S
RX J1749.3+6737	2990	17 49 18.0	+67 37 29	11.503	11.030	10.864	K5e	N
RX J1749.9+6611	3040	17 49 55.9	+66 11 08	12.099	11.474	11.298	M0e	G,N
RX J1750.2+6207	3070	17 50 15.0	+62 07 56	10.066	9.657	9.522	K4	G,N
RX J1750.4+7045	3080	17 50 25.3	+70 45 36	7.704	7.120	6.961	K2.5	S
RX J1751.8+6414	3161	17 51 49.2	+64 15 01	10.679	10.195	10.062	K4-5	G
RX J1752.7+6700	20	17 52 44.8	+67 00 20	8.571	8.130	8.034	G8+F6+F0	N
RX J1752.7+6738	30	17 52 44.6	+67 38 31	10.563	10.113	9.983	K4	N
RX J1752.7+6804	31	17 52 45.6	+68 05 00				M3	G
RX J1752.9+6625	3220	17 52 56.0	+66 25 10	6.103	5.671	5.566	K0	S
RX J1753.8+6852	3270	17 53 51.5	+68 52 28	10.746	10.149	10.077	K0	G
RX J1754.1+6948	3310	17 54 07.8	+69 48 26	10.894	10.591	10.492	G5	G
RX J1756.2+6807	3500	17 56 14.0	+68 07 09	10.481	9.888	9.775	M0e	N
RX J1757.0+6849	3560	17 57 03.7	+68 49 14	7.733	7.423	7.361	G8	N
RX J1757.2+6547	190	17 57 14.3	+65 46 58	11.991	11.304	11.110	M3e	G,N
RX J1758.0+6409	3610	17 58 01.4	+64 09 34	8.365	7.859	7.737	K4	N

Table 2. continued.

Name	Scan	RA(J2000) (h m s)	Dec(J2000) ° ′ ″	*J*	*H*	*K*	Sp.	Note
RX J1758.3+6735	240	17 58 18.9	+67 35 15	12.979	12.374	12.071	M4e	G,N
RX J1758.4+6726	260	17 58 28.3	+67 26 08	9.327	9.069	9.005	G2	N
RX J1758.7+6350	3690	17 58 48.0	+63 50 39	8.107	8.022	7.980	A2	S
RX J1758.9+6211	281	17 58 54.1	+62 11 24	15.973	15.455	14.996	M2	G
RX J1759.2+6408	3710	17 59 13.8	+64 08 33	6.480	6.323	6.315	F2	S
RX J1759.3+6602	330	17 59 23.6	+66 02 55	8.699	8.215	8.114	G9	N
RX J1800.0+6645	370	18 00 02.2	+66 45 53	9.711	9.460	9.375	F8	N
RX J1800.1+6835	3790	18 00 10.0	+68 35 56	15.501	15.930	15.443	WD†	S
RX J1800.3+6349	3800	18 00 24.3	+63 49 53	10.417	9.819	9.616	M0	G
RX J1800.9+6600	470	18 00 57.4	+66 00 56	11.780	11.211	11.104	K4	G
RX J1801.3+6654	500	18 01 21.9	+66 54 04	10.049	9.522	9.395	K3+K4	N
RX J1801.4+6800	501	18 01 26.7	+68 00 30	11.849	11.291	11.166	K5e	N
RX J1802.2+6415	3900	18 02 15.2	+64 16 03	8.541	7.962	7.652	M4e	N
RX J1803.0+6445	3970	18 03 05.8	+64 45 29	11.328	10.690	10.490	M4/5	G
RX J1803.4+6437	3990	18 03 33.6	+64 37 47	11.713	11.098	10.797	G2	G
RX J1804.2+6754	680	18 04 14.0	+67 54 11	12.882	12.265	12.060	CV†	S
RX J1804.3+6629	700	18 04 24.7	+66 29 28	16.117	15.309	15.596	Hot SD†	G
RX J1804.5+6429	4010	18 04 32.9	+64 29 03	10.810	10.203	9.935	M8	G
RX J1804.6+6528	4121	18 04 38.6	+65 28 58	11.614	11.265	11.133	K4	G
RX J1805.1+6353	4060	18 05 08.4	+63 53 35	11.650	11.039	10.849	M2e	G
RX J1805.5+6945	4090	18 05 30.5	+69 45 17	9.534	9.251	9.143	G2	G
RX J1805.5+6219	4100	18 05 30.3	+62 19 03	6.536	6.167	6.044	K0	S
RX J1805.7+6551	4130	18 05 44.8	+65 51 58	8.494	8.308	8.240	F5	S
RX J1806.3+6524	4160	18 06 21.8	+65 24 06	11.867	11.334	11.222	K4	G
RX J1806.6+6413	4180	18 06 41.0	+64 13 18	4.980	4.435	4.364	K0	S
RX J1806.7+6822	4190	18 06 43.6	+68 22 01	9.685	9.064	8.845	M4e	N
RX J1806.7+6626	750	18 06 47.0	+66 26 07	16.511	16.119	15.136	M0	G
RX J1807.0+6643	4211	18 06 58.2	+66 43 30	16.610	15.936	15.703	K5	G
RX J1807.3+6635	4240	18 07 19.9	+66 35 29	10.535	9.995	9.855	K5e	N
RX J1807.6+6829	4260	18 07 39.7	+68 29 22	10.922	10.472	10.350	K4	G
RX J1808.4+6437	4281	18 08 23.7	+64 37 12	11.254	10.642	10.487	M0e	G
RX J1808.5+6643	4310	18 08 35.3	+66 43 22	11.930	11.394	11.270	K4e	N
RX J1808.6+6735	4350	18 08 41.6	+67 36 00	10.282	9.768	9.675	K2	G
RX J1808.7+6256	4380	18 08 45.4	+62 56 37	7.082	6.708	6.619	G5	S
RX J1809.9+6940	4470	18 09 55.8	+69 40 39	6.872	6.455	6.326	K3	N
RX J1810.1+6728	4500	18 10 08.0	+67 28 35	10.452	10.040	9.973	K0	N
RX J1810.8+7016	4530	18 10 49.9	+70 16 09	9.183	8.810	8.679	G9	G
RX J1811.3+6314	4570	18 11 21.5	+63 14 49	11.447	11.130	11.021	K0	N
RX J1812.7+6533	4650	18 12 44.6	+65 33 49	10.131	9.680	9.567	K2	N
RX J1812.8+6946	4660	18 12 54.3	+69 46 23	12.502	11.906	11.667	M4	G
RX J1813.7+6628	4750	18 13 47.0	+66 28 59	16.191	15.474	14.983	M2	N
RX J1813.7+6707	4770	18 13 45.9	+67 07 41	12.275	11.771	11.647	K2e+K2	G
RX J1813.8+6831	4780	18 13 48.6	+68 31 32	8.882	8.310	8.177	K2	N
RX J1813.8+6423	4810	18 13 51.4	+64 23 57	4.203	4.059	3.944	F5	S
RX J1816.2+6529	4931	18 16 21.2	+65 29 39	5.500	4.726	4.513	K8	N
RX J1816.5+6547	4960	18 16 32.3	+65 47 02	12.263	11.646	11.529	K4e	G
RX J1816.8+6504	4970	18 16 49.7	+65 04 26	9.130	8.669	8.544	K2	N
RX J1816.9+6449	4980	18 16 58.6	+64 49 34	11.256	11.017	10.952	G2	N
RX J1818.5+7042	5060	18 18 31.9	+70 42 17	8.816	8.424	8.418	G5	S
RX J1818.9+6611	5090	18 18 53.7	+66 11 54	8.740	8.264	7.948	M5e	G
RX J1819.9+6636	5170	18 19 53.8	+66 36 19	12.932	12.605	12.532	G4	G
RX J1820.3+6519	5220	18 20 19.2	+65 19 19	6.967	6.772	6.712	F8	S
RX J1821.3+6559	5280	18 21 25.0	+65 59 31	10.037	9.386	9.201	M3e	G
RX J1821.7+6357	5320	18 21 46.8	+63 57 10	8.373	8.052	7.988	K0	N
RX J1823.1+6533	5380	18 23 06.8	+65 33 14	9.019	9.028	8.996	A2	G
RX J1823.4+6257	5410	18 23 26.7	+62 57 18	11.367	10.943	10.892	G5+K3/4	N
RX J1824.5+6349	5480	18 24 29.6	+63 49 37	12.882	12.637	12.571	M0	G
RX J1824.7+6509	5500	18 24 47.3	+65 09 25	15.518	14.741	13.611	AGN†	N
RX J1825.1+6450	5510	18 25 09.0	+64 50 21	5.052	4.743	4.362	K4	G,N

Table 2. continued.

Name	Scan	RA(J2000) (h m s)	Dec(J2000) ° ′ ″	*J*	*H*	*K*	Sp.	Note
RX J1825.5+6234	5520	18 25 32.9	+62 34 15	8.394	7.896	7.721	K4e	N
RX J1827.9+6235	5600	18 27 57.0	+62 35 41	10.584	9.916	9.728	M0e	G
RX J1828.5+6322	5660	18 28 32.2	+63 21 59	11.295	10.858	10.751	K4	G, N
RX J1829.3+6409	5710	18 29 17.6	+64 09 17	13.078	12.753	12.497	M3e+M3	G, N
RX J1829.3+6751	5711	18 29 20.6	+67 51 33	11.948	11.456	11.354	K4e	G
RX J1829.5+6905	5730	18 29 31.7	+69 05 13	10.621	10.152	10.036	G5	G
RX J1829.7+6435	5760	18 29 46.1	+64 35 20	10.893	10.691	10.645	F8+K1	G, N
RX J1831.1+6214	5840	18 31 04.5	+62 14 39	11.749	11.495	11.444	F8	N
RX J1831.3+6454	5860	18 31 21.7	+64 54 11	9.360	8.796	8.533	M4e	G
RX J1831.7+6511	5880	18 31 44.4	+65 11 32	15.678	15.144	14.960	Be†	G
RX J1832.0+7002	5910	18 32 03.9	+70 02 41	9.792	9.153	8.773	M2e+M3	N
RX J1832.5+6836	5950	18 32 29.5	+68 36 52	6.590	6.394	6.353	G0	N
RX J1833.5+6431	5992	18 33 29.2	+64 31 54	14.098	13.516	13.241	M2e	G
RX J1833.6+6259	6010	18 33 38.2	+62 59 26	10.406	10.053	9.991	F8	G
RX J1833.8+6513	6030	18 33 47.8	+65 13 33	7.710	7.247	7.124	K3	N
RX J1834.1+6438	6060	18 34 08.2	+64 38 25	11.441	10.865	10.539	M5e	G
RX J1834.5+6931	6051	18 34 33.6	+69 31 45	10.079	9.630	9.533	G5	G
RX J1835.8+6446	6140	18 35 50.7	+64 46 07	11.634	10.985	10.756	M6	G
RX J1835.9+6336	6150	18 35 53.7	+63 36 53	14.707	14.328	14.322	G5	G, N
RX J1836.2+6529	6160	18 36 13.5	+65 29 15	5.426	5.396	5.314	F0	S
RX J1836.3+6654	6163	18 36 22.8	+66 54 54	6.403	6.140	6.092	G3	S
RX J1836.9+6747	6210	18 36 55.7	+67 47 09	11.137	10.784	10.718	F6	G
RX J1837.5+6231	6240	18 37 33.6	+62 31 31	5.725	5.773	5.753	A0	S
RX J1839.4+6903	6350	18 39 25.4	+69 02 54	8.533	7.881	7.676	M3e	N
RX J1839.8+6537	6370	18 39 47.5	+65 37 59	10.409	10.055	9.959	K3	N
RX J1840.5+6521	6390	18 40 33.6	+65 21 37	11.319	10.676	10.541	M0e	G
RX J1840.7+7038	6400	18 40 44.4	+70 38 47	8.043	7.669	7.563	K2	N
RX J1840.9+6245	6410	18 40 56.6	+62 44 54	4.645	4.139	4.061	K0III	S
RX J1840.9+6528	6420	18 40 58.6	+65 28 34	11.764	11.095	10.915	K7e	G
RX J1841.9+6316	6451	18 41 57.8	+63 16 26	9.998	9.436	9.234	M4e	G
RX J1843.2+6956	6510	18 43 12.6	+69 55 54	8.585	8.376	8.334	F0	S
RX J1843.7+6514	6530	18 43 46.0	+65 14 08	10.367	9.713	9.531	M2e	N
RX J1844.2+6719	6541	18 44 14.6	+67 19 33	11.585	10.947	10.703	M5e	G
RX J1844.6+6338	6545	18 44 39.1	+63 38 28	10.851	10.509	10.441	G2	G

† Discarded from the sample of "normal stars".
Notes: S (Spectral type from SIMBAD), G (Spectra from Gioia et al. 2003), N (Spectra obtained in this work with the NOT telescope.